Imaging by electromagnetic induction with resonant circuits

Roberta Guilizzoni[a], Joseph C. Watson[b], Paul Bartlett[a], Ferruccio Renzoni[a]
[a]Department of Physics & Astronomy, University College London, Gower Street, London, WC1E 6BT, United Kingdom; [b]Novel Detection Concepts, National Nuclear Security Programme, Atomic Weapons Establishment, Aldermaston, Reading, RG7 4PR, United Kingdom

ABSTRACT

A new electromagnetic induction imaging system is presented which is capable of imaging metallic samples of different conductivities. The system is based on a parallel LCR circuit made up of a cylindrical ferrite-cored coil and a capacitor bank. An AC current is applied to the coil, thus generating an AC magnetic field. This field is modified when a conductive sample is placed within the magnetic field, as a consequence of eddy current induction inside the sample. The electrical properties of the LCR circuit, including the coil inductance, are modified due to the presence of this metallic sample. Position-resolved measurements of these modifications should then allow imaging of conductive objects as well as enable their characterization. A proof-of-principle system is presented in this paper. Two imaging techniques based on Q-factor and resonant frequency measurements are presented. Both techniques produced conductivity maps of 14 metallic objects with different geometries and values of conductivity ranging from 0.54×10^6 to 59.77×10^6 S/m. Experimental results highlighted a higher sensitivity for the Q-factor technique compared to the resonant frequency one; the respective measurements were found to vary within the following ranges: $\Delta Q=[-11,-2]\%$, $\Delta f=[-0.3,0.7]\%$. The analysis of the images, conducted using a Canny edge detection algorithm, demonstrated the suitability of the Q-factor technique for accurate edge detection of both magnetic and non-magnetic metallic samples.

Keywords: Imaging, electromagnetic induction, eddy currents, material characterization.

1. INTRODUCTION

Electromagnetic induction imaging[1-6] has wide application in diverse fields such as medicine[1-2], security[3], industry[6], archaeology and geophysics. For instance, it has been largely exploited for crack detection of industrial materials and characterization of their level of corrosion. Electromagnetic induction imaging presents some advantages in comparison to other existing imaging techniques, being non-invasive and contactless. Furthermore, it is sensitive to all electromagnetic properties of materials: conductivity, permittivity and permeability.

In the past few years, significant effort has aimed at developing high-sensitivity methods for the detection and imaging of metallic objects. Among the different realizations, we recall here a recent high-sensitivity method based on the measurement of the Q-factor, developed to detect and image steel reinforcing bars embedded in concrete[7], in order to monitor their condition and provide information about the health of the concrete structure. Q-detection sensors, incorporating digital signal processing, have been exploited since the introduction of metal detectors. These sensors' working principle is based on the increase of impedance of a coil which occurs whenever a conductive object is inductively coupled to it. This phenomenon is due to eddy current production inside the sample. The Q-factor of a coil within a tuned system drops when high-conductivity targets of low permeability are exposed to the changing magnetic field generated by the coil. However, purely permeable targets cause an increase of Q-factor. Q-detection sensors are part of a wider family of inductive sensors. High-sensitivity detection methods based on the use of inductive sensors are object of intense research. For instance, these sensors have been recently used for detection of metallic wear debris[8-9] aimed at condition monitoring of rotating and reciprocating machinery. A high-sensitivity method based on an inductance-capacitance resonance system was developed to this purpose[8]. The amplified impedance change at resonance, due to the presence of a wear debris particle, could be exploited to detect metallic specimens ranging from 32 to 172 μm.

In the present work, a new measurement system is reported, based on a resonant LCR circuit, which has shown promising results for 2D imaging of metallic samples spanning conductivity values from 0.54×10^6 to 59.77×10^6 S/m, plus the ability to undertake material characterization. Images of 14 conductive materials, inductively coupled to a ferrite-cored coil, were obtained via position-resolved measurements of the resonant frequency and Q-factor associated

Image Sensing Technologies: Materials, Devices, Systems, and Applications II, edited by Nibir K. Dhar, Achyut K. Dutta, Proc. of SPIE Vol. 9481, 94810Q

to the resonating system. It is demonstrated that the proposed Q-factor method provides clear images of both magnetic and non-magnetic metallic samples of all conductivities, and can be used for material characterization.

2. MATERIALS AND METHODS

2.1 Description of the experimental apparatus

The experimental system is based on a cylindrical ferrite-cored coil in which an AC primary magnetic field is induced. The coil is connected in parallel to a capacitor selected from a capacitor bank. Together with the internal components' internal resistance, this forms an LCR resonating system. In the following, this will be modeled as a parallel LCR circuit. Both the coil and capacitor bank are connected to an impedance analyzer (Wayne Kerr 6500 B). A metallic specimen is secured on a two-axis XY stage inserted into a wooden support structure having non-metallic fixtures (Figure 1). The support structure was created in such a way as to allow positioning of the specimen at different lift-offs (i.e. vertical distances from the coil lower base to the samples).

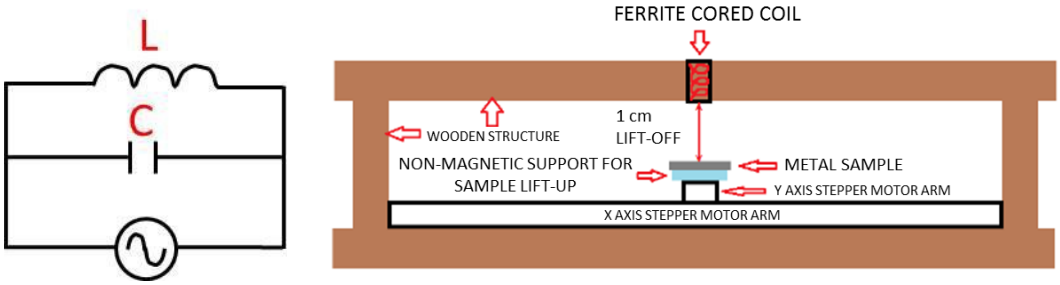

Figure 1. Left: Electronic schematic of the system, which consists in a parallel LC circuit made up of a ferrite-cored coil (No. turns=145±1, Ø=7.8±0.5 mm, height=9.5±0.5mm, inductance=680.0±0.1 μH), and a capacitor selected from a capacitor bank. Right: Sketch of the wooden structure built in order to perform scanning of metallic samples.

2.2 Description of the procedure used for 2D imaging of metallic objects

A new method has been developed to achieve 2D imaging of metallic objects by means of the resonating circuit described in Section 2.1. First, a technique based on resonant frequency measures has been tested by applying the procedure which is described in the next paragraph. Second, a similar procedure has been used to obtain Q-factor measurements. Experimental results obtained with the two techniques are reported and discussed in Sections 3.1-3.4.

The methods utilize a computer automated system which links, via Ethernet connections, a PC, the impedance analyzer and a two-axis stepper motor. A Labview Virtual Instrument (VI) was created to control the stepper motor movements as well as the data acquisition undertaken by the impedance analyzer. A timed sequence structure was created to perform the following operations: 1) move the metallic sample along the first row of the scanning area in 2.5-mm-steps; 2) stop the sample at each position and activate the impedance analyzer; 3) perform a frequency sweep of the impedance amplitude in a frequency interval centered around the system's resonant frequency; 4) deactivate the impedance analyzer and move the sample one step ahead; 5) repeat operations 1)-4) for all rows of the scanning area.

The following mathematical operations were undertaken in order to determine the values of resonant frequency and Q-factor to be used to generate tomographic images. Impedance amplitude values (Z) were plotted against the corresponding angular frequency values (ω) at each positional point along the scanning area. Measured Z vs ω curves showing the resonant peak at each position were thus obtained for all positional data. Each of these curves was fitted using the function for the impedance for a parallel LCR circuit:

$$Z(\omega) = \frac{1}{\sqrt{\left(\frac{1}{R}\right)^2 + \left(\frac{1}{\omega L} - \omega C\right)^2}}, \qquad (1)$$

setting R, L and C as the fit parameters.

The parameters obtained from the fit were used to calculate the Q-factor by means of the formula:

$$Q = R\sqrt{\frac{C}{L}}\ . \qquad (2)$$

A value of Q-factor was thus obtained at each position of the specimen. In a similar way, values of the resonant frequency at each position of the specimen were determined by using the formula:

$$f = \frac{1}{2\pi\sqrt{LC}}, \qquad (3)$$

where *L* and *C* were derived from the fit.

Background measurements of resonant frequency and Q-factor were first taken at each position of the explored area with the coil in air. Sample data were then taken after placing the metal object under the coil. Normalized data were obtained by dividing each sample data by the corresponding background data. 2D surface plots were generated by means of interpolation with a piecewise cubic fit, by plotting normalized data against the x and y coordinates of the imaged sample.

2.3 Study of the influence of lift-off on the resonant frequency and Q-factor measurements

A preliminary study was carried out in order to investigate the possibility of generating good quality images of metallic samples by means of two contactless imaging techniques based on resonant frequency and Q-factor measurements, respectively. The dependence of the quality of the image on the lift-off (*L*) was studied by means of two experiments. The first one consisted in measuring the system's resonant frequency and Q-factor when a squared aluminum sample- having edge equal to (25±1)mm and thickness equal to (1.0±0.1)mm (Table 1)- was placed under a ferrite-cored coil. The following values of lift-off were arbitrarily chosen: L_1=(6.0±0.1)cm; L_2=(2.0±0.1)cm; L_3=(1.5±0.1)cm; L_4=(1.0±0.1)cm and L_5=0 cm. The second experiment applied the procedures described in Section 2.2 to investigate the aluminum sample at each lift-off. This part of the work aimed at supporting the observations obtained from the first experiment.

2.4 Imaging of high-conductivity samples made of copper and aluminum

The method described in Section 2.2 was initially tested with high-conductivity metallic samples. Disk samples having diameter *D*=(2.00±0.05)cm and thickness *t*=(2.0±0.5)mm (Table 2), made of copper and aluminum, were used for this purpose. A 4.25x4.25 cm^2 area was scanned by moving each sample along a plane parallel to the coil lower base. The lift-off was equal to (1.0±0.1)cm and the capacitance was set to C=(1.0000±0.0001)μF.

Copper and aluminum samples having dimensions 25x25x1 mm^3 were also imaged, in order to investigate the ability of the system to resolve shapes.

2.5 Material characterization: comparison between resonant frequency and Q-factor techniques

Lower conductivity metals were included in the study in order to investigate whether the proof-of-principle proposed could be extended to metals spanning a wide range of conductivities. The results of the previous experiments highlighted the need for a new method enabling material characterization. In order to investigate the system's behavior further, a quantitative analysis was performed by measuring the resonant frequency and Q-factor change due to the presence of 14 representative metallic samples of different conductivities. The samples used are listed in Table 1.

The changes in resonant frequency and Q-factor values, due to the presence of a metallic object, were calculated by using the following formulas:

$$\Delta f\ (\%) = \frac{f(metal) - f(air)}{f(air)}\ (\%) \qquad (4)$$

$$\Delta Q\ (\%) = \frac{Q(metal) - Q(air)}{Q(air)}\ (\%) \qquad (5)$$

where *f(metal)* and *Q(metal)* represent the resonant frequency and Q-factor values measured when the metallic sample was placed under the coil (1 cm lift-off); *f(air)* and *Q(air)* are values measured in air.

The described procedure was repeated with a value of lift-off L=0 cm. The change in Q-factor plotted against conductivity was compared for data obtained at L=(1.0±0.1)cm and L=0 cm. This experiment aimed at identifying a procedure which allowed to distinguish between high-conductivity samples.

Table 1. List of 25x25x1mm^3 14 metals included in the study with the purpose of material characterization.

Metal	σ (10^6 S/m)[10]
Copper (Cu)	59.77
Gold (Au)	42.55
Aluminum (Al)	37.67
Zinc (Zn)	16.9
Iron (Fe)	10.3
Tin (Sn)	9.09
Niobium (Nb)	8
Tantalum (Ta)	8.03
Lead (Pb)	4.84
Vanadium (V)	4.03
Hafnium (Hf)	2.85
Titanium (Ti)	2.38
Bismuth (Bi)	0.94
Manganese (Mn)	0.54

Table 2. List of copper and aluminum disks of different diameters and thicknesses included in the study to investigate imaging of high-conductivity samples.

Metal	diameter (mm)	thickness (mm)
Copper	15.0±0.5	2.0±0.5
Copper	17.0±0.5	2.0±0.5
Copper	20.0±0.5	2.0±0.5
Copper	30.0±0.5	2.0±0.5
Copper	30.0±0.5	0.7±0.5
Aluminum	15.0±0.5	2.0±0.5
Aluminum	17.0±0.5	2.0±0.5
Aluminum	20.0±0.5	2.0±0.5
Aluminum	30.0±0.5	2.0±0.5

2.6 Edge estimation with resonant frequency and Q-factor techniques

A resolution study was conducted in order to detect the edge and diameter of the samples. This was accomplished by means of a Canny edge detection algorithm[11] that enabled the edge of the images to be detected. The results achieved by using the resonant frequency and Q-factor techniques, with the external capacitance set to two arbitrary values (C=1 μF and C=0.5 μF) were compared. This quantitative analysis aimed at comparing both the ability to resolve shapes of the resonant frequency and Q-factor techniques and the system's behavior when different values of capacitance were used.

3. RESULTS AND DISCUSSION

3.1 Study of the influence of lift-off on the resonant frequency and Q-factor measurements

The results of the study about the dependence of the measured quantities on the lift-off are summarized in Figure 2. The graph in this figure shows the values of resonant frequency and Q-factor normalized to background values plotted against lift-offs.

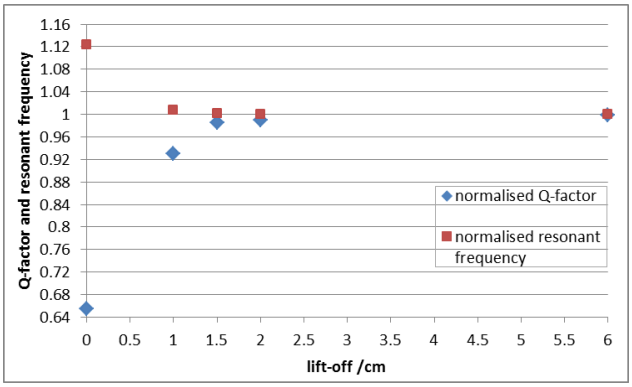

Figure 2. Normalized Q-factor (blue) and resonant frequency (red) plotted against lift-off (cm).

As shown by Figure 2, the Q-factor curve saturates at values of lift-off higher than 2 cm, whereas the resonant frequency curve saturates at L=1.5 cm. The images of the aluminum sample obtained for each value of lift-off show good reproduction of the sample's shape and size at L<6 cm for both resonant frequency and Q-factor measurements. It was established that an optimal lift-off would be the result of a trade-off between good reproduction of the shape and size of the imaged object and the need for a contactless technique. Based on this consideration, the lift-off chosen for the future experiments was L=1 cm.

3.2 Imaging of high-conductivity samples made of copper and aluminum

Images of a 2-mm-thick, 2-cm-diameter aluminum disk, obtained via position-resolved measurements of the resonant frequency and of the Q-factor, are shown in Figure 3.

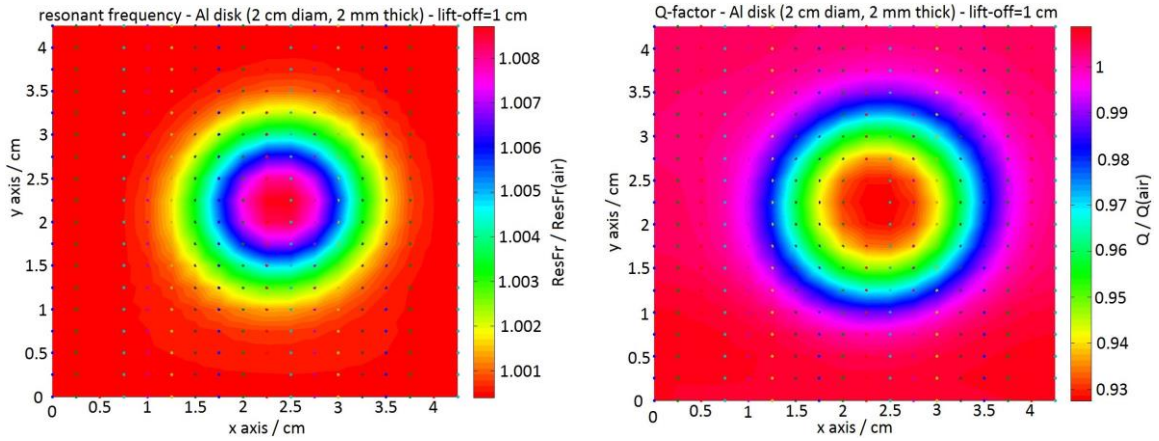

Figure 3. 2-cm-diameter aluminum disk sample imaged via position-resolved measurements of the resonant frequency (left) and of the Q-factor (right). The resonant frequency and Q-factor- measured at the center of the object and normalized to the value in air- were equal to f_r=1.009 and Q=0.93.

Figure 3 shows that the imaged samples are distinguishable from the background. Both their shape and size compare very well with the actual ones. Similar images to those shown in Figure 3 were obtained with copper samples. The normalized resonant frequency and Q-factor values measured at the center of the object were equal to f_r=1.009 and Q=0.94, respectively.

Figure 4 shows surface plots obtained with a 25x25x1mm^3 copper sample after setting the capacitance to C=0.5 μF.

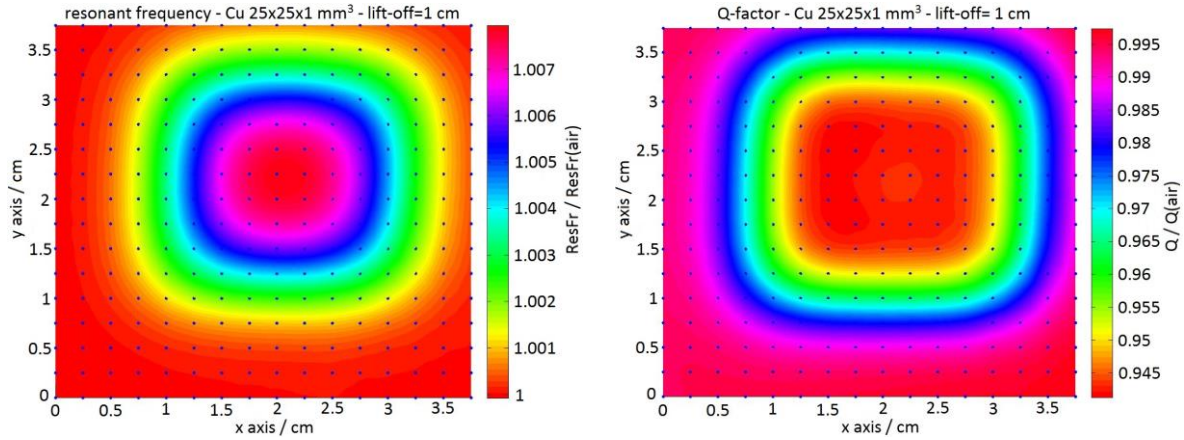

Figure 4. Image of a 25x25x1mm^3 copper sample obtained via position-resolved measurements of the resonant frequency (left) and the Q-factor (right). The normalized resonant frequency and Q-factor at the center of the sample were equal to f_r=1.008 and Q=0.94.

Similar images were obtained with an aluminum sample having the same geometry as the copper one. The normalized resonant frequency and Q-factor at the center of the sample were equal to f_r=1.007 and Q=0.93, respectively. These results demonstrated the suitability of both resonant frequency and Q-factor methods to 2D imaging of high-conductivity samples of different shapes. At this stage, neither images of disks nor images of squared samples were able to distinguish between the two metals.

3.3 Material characterization: comparison between resonant frequency and Q-factor techniques

Figure 5 shows the result of the quantitative analysis which aimed at investigating the possibility to characterize materials of different conductivities. Changes in resonant frequency and Q-factor are plotted against the metal's conductivity[10].

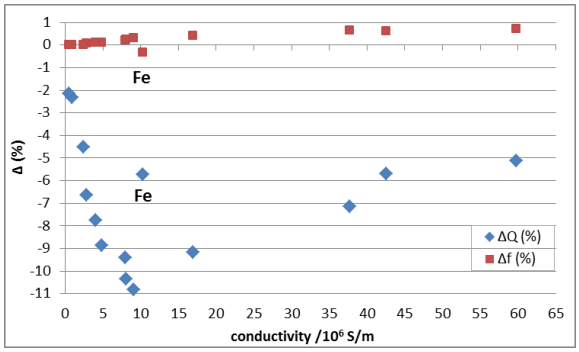

Figure 5. Change in Q-factor and resonant frequency plotted against metal's conductivity[11]. The physical quantities were measured at C=1 μF.

In both the red and blue curves in Figure 5, the point corresponding to the conductivity value of iron (σ_{Fe}=10.3x10^6 S/m) does not follow the general data trend. The different behavior of this metal is accounted for its ferromagnetic nature, which is responsible for an increase in the magnetic flux density. Figure 5 shows that the Q-factor varies in a much wider interval than the resonant frequency: ΔQ=[-11, -2]%, Δf=[-0.3, 0.7]%. Leaving aside the data points corresponding to iron, both the red and blue curves have a well-defined trend.

Plots similar to the ones shown in Figure 5 were obtained by setting the capacitance to C=0.5 μF. In this case, Q-factor and resonant frequency varied with conductivity within a range equal to ΔQ=[-15, -3.8]%, Δf=[-0.25, 0.67]%. These results imply that the system's behavior is the same if the external capacitance value is changed, and generalized conclusions can thus be drawn.

Due to the shape of the blue curve, each value of Q-factor is not univocally related to a metal of certain conductivity. Therefore, different metals cannot be distinguished from each other by simply measuring the Q-factor. On the other hand, the resonant frequency trend (red curve) is represented by a monotonic function. This clearly shows the potential of this technique to achieve the goal of material characterization. However, higher change of resonant frequency than the one obtained is required.

The following observations can be made about the system's behavior in the regions corresponding to the limits of low and high conductivity (σ):

1) σ from 0.54 to 4.03x10^6 S/m (low-conductivity metals: Hf, Ti, Bi, Mn). The Q-factor change shows a large variation with conductivity for low conductivity metals. On the other hand, samples with low-conductivity (particularly, bismuth and manganese) produce a negligible change of resonant frequency of the circuit. This result is confirmed by images of manganese and bismuth shown in Figure 6, in which the imaged samples cannot be well distinguished from the background. Corresponding images obtained via position resolved measurements of the Q-factor show that the samples are very well distinguished from the background by means of the Q-factor technique (Figure 7).

2) σ from 37.67 to 59.77x10^6 S/m (high-conductivity metals: Al, Au, Cu). The Q-factor saturates at high conductivities. This explains the difficulty of producing different images of copper and aluminum samples.

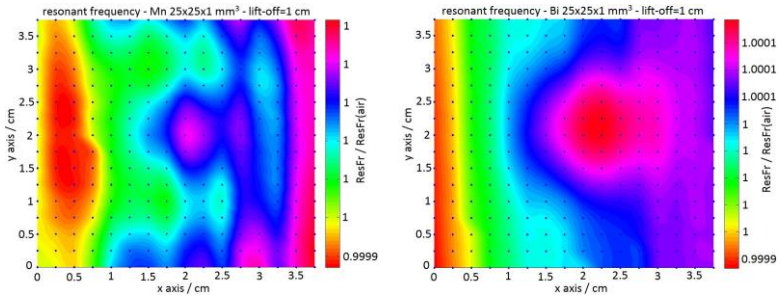

Figure 6. Images of 25x25x1mm^3 manganese (left) and bismuth (right) samples obtained via position-resolved measurements of the resonant frequency, for a capacitance C=1 μF. Due to the small change of resonant frequency from the background value, it is not possible to visualize the manganese object. Although the change of resonant frequency from the background value for bismuth is bigger than that obtained with lower-conductivity manganese, the object cannot be clearly distinguished from the background.

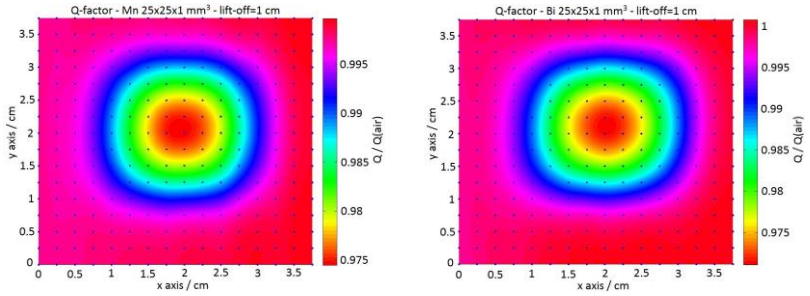

Figure 7. Images of 25x25x1mm^3 manganese (left) and bismuth (right) samples obtained via position-resolved measurements of the Q-factor, for a capacitance C=1 μF. The samples can be seen in this case.

The results shown in Figure 7 imply that the Q-factor imaging technique provides higher sensitivity than the resonant frequency imaging technique. The Q-factor imaging technique allows characterizing materials having similar values of conductivity and allows imaging over a broad range of conductivity.

The system's behavior corresponding to the limits of both low and high conductivity was investigated further.

- In the case of low-conductivity metals, the capacitance value was reduced from C=1 μF to C=0.5 μF. The aim of this experiment was to see whether it could be possible to visualize the objects by modifying the circuit's capacitance and, therefore, its resonant frequency. Images of manganese and bismuth samples were obtained by means of resonant frequency measurements (Figure 8). We observe that, in this case, the objects can be distinguished from the background, unlike what occurred at C=1 μF. This is due to the non-linear rate of change of the resonant frequency with the capacitance. These results demonstrate that resonant frequency imaging of low conductivity objects is possible by selecting an appropriate value of capacitance. However, this implies that the resonant frequency imaging method is restricted to only certain values of capacitance. On the other hand, the sensible change of Q-factor at all capacitance values makes imaging of all conductivity samples possible, irrespective of the capacitance.

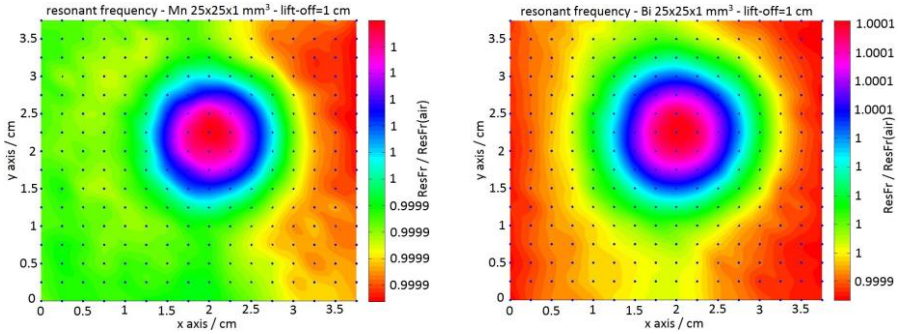

Figure 8. Image of 25x25x1mm^3 manganese (left) and bismuth (right) samples obtained via position-resolved measurements of the resonant frequency, for a capacitance C=0.5 μF. The imaged samples are now visible due to the sensible change of resonant frequency produced by a lower capacitance.

- In the case of high-conductivity samples, an experiment was conducted to try to overcome the issue linked to Q-factor saturation at high conductivities. As suggested by the trend of the blue data shown in Figure 1, Q-factor change measured with aluminum strongly increases at values of lift-off lower than 1 cm. In order to extend this result to all conductivity metals, the Q-factor change was measured for each sample at 1-cm-lift-off and 0-cm-lift-off (Figure 9).

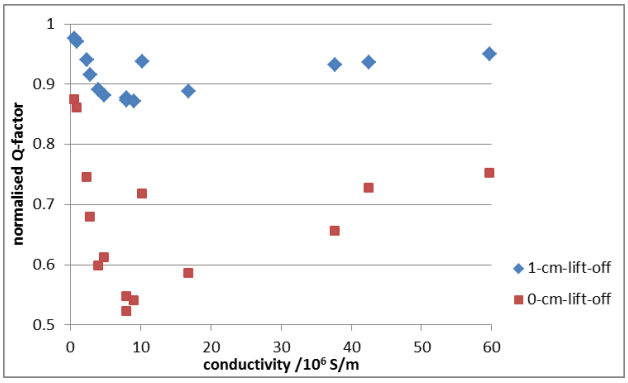

Figure 9. Normalized Q-factor plotted against conductivity, at lift-off=1 cm and lift-off=0.

Figure 9 explains why it was not possible to distinguish between a copper and an aluminum sample by using the Q-factor technique at 1-cm-lift-off. The choice of an intermediate value of lift-off, equal to L=0.5 cm, successfully distinguished the two metals from each other with the Q-factor technique. The change of Q between the two metals was calculated as:

$$\Delta Q\ (\%) = \frac{Q(Cu) - Q(Al)}{Q(Al)}\ (\%), \tag{6}$$

where Q(Cu) and Q(Al) were Q-factor values measured at the center of the image of copper and aluminum sample, respectively. This value was found equal to ΔQ = (-44.11±0.06) %. In comparison, the change of resonant frequency, calculated with the formula:

$$\Delta f\ (\%) = \frac{f(Cu) - f(Al)}{f(Al)}\ (\%), \tag{7}$$

was found equal to Δf = (0.38±0.04)%, .

Images of copper and aluminum squared samples at L=0.5 cm confirmed that the two metals produced different images and could thus be differentiated.

3.4 Edge estimation with resonant frequency and Q-factor techniques

The results of the resolution study conducted with an aluminum sample by using the Canny edge detection algorithm[11] are shown in Figure 10.

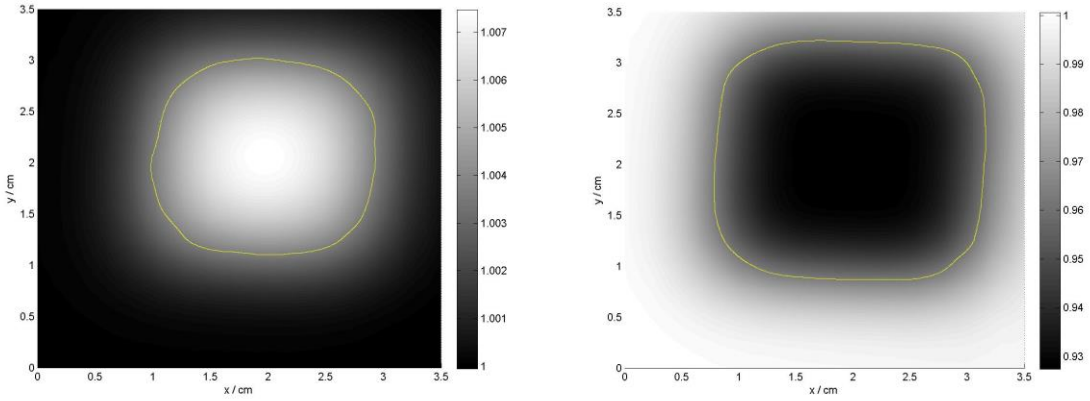

Figure 10. Canny edge detection algorithm applied to gray scale image of aluminum metallic sample (25x25x1 mm^3), obtained with resonant frequency imaging technique (left) and Q-factor imaging technique (right), for a capacitance C=1 μF.

Figure 10 shows that the shape of the sample is best reproduced with the Q-factor technique. This is confirmed by Figure 11, in which the ratio between detected edge (L_{meas}) and 'real' one (L_{real}) is plotted against the metal's conductivity. This figure shows that the edge estimation improves when the metal's conductivity is increased. This is due to the increase of inductance change with conductivity, causing the measured physical quantities to differ from the background quantities by a larger amount. For this reason, the Q-factor technique provides a very good estimate of the edge of high-conductivity metals like copper, gold and aluminum.

Interestingly, the edge underestimation highlighted by the blue data in Figure 11 can be corrected by applying a correction factor to it. The correction factor was derived by dividing the data reported in the red curve by the ones reported in the blue curve, excluding the data points corresponding to iron.

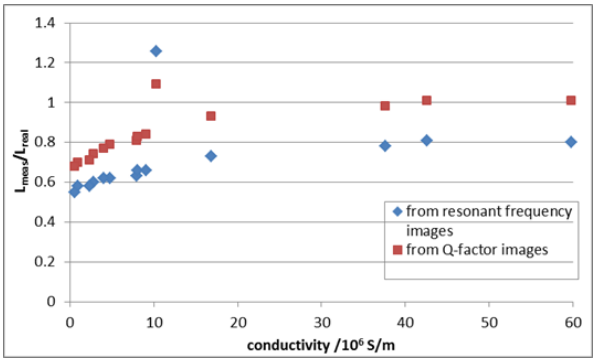

Figure 11. Ratio between measured edge and actual edge of the sample, plotted against conductivity. Edge values were estimated from the images obtained with a capacitance C=0.5 μF. Blue dots represent data obtained using the resonant frequency imaging technique, whereas red dots represent data obtained using the Q-factor imaging technique.

The results obtained with copper and aluminum disks are reported in Figure 12, where the estimated diameter is plotted against the actual diameter.

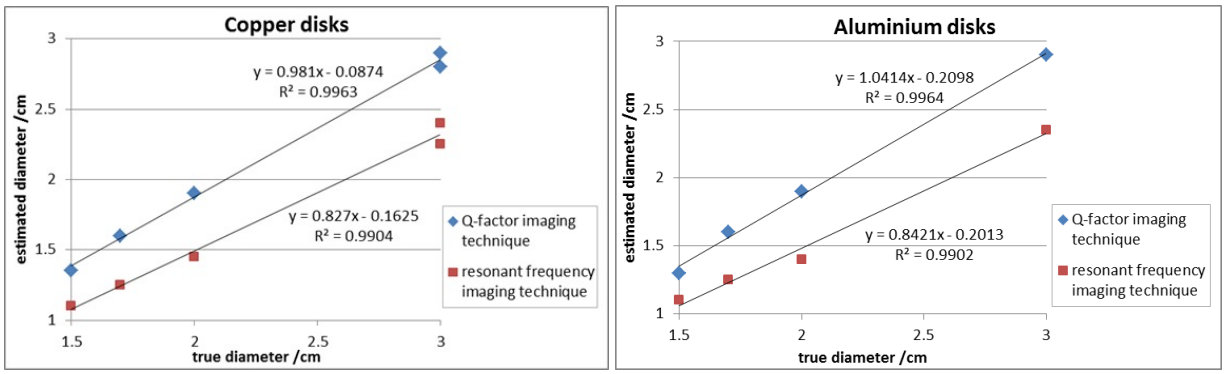

Figure 12. Estimated diameter vs actual diameter for 1.5, 1.7, 2 and 3 cm diameter copper (left) and aluminum (right) disks. The two points corresponding to 3 cm refer to copper samples of thicknesses equal to 0.7 mm and 2 mm. The trend obtained with the Q-factor technique (blue) is linear, as well as the trend obtained with the resonant frequency technique (red).

Figure 12 shows that it is possible to determine the actual diameter (D_t) from the one estimated with the Canny edge algorithm (D_e). In particular, the following formulas can be used for copper and aluminum samples:

$$D_t(Cu) = \frac{D_e(Cu) + 0.0874}{0.981} \tag{8}$$

$$D_t(Al) = \frac{D_e(Al) + 0.2098}{1.0414} \tag{9}$$

Graphs similar to those shown in Figure 12 were obtained at C=0.5 μF, therefore the sample's diameter can be estimated by using formulas similar to (8) and (9) that can be derived from linear fits of data.

4. CONCLUSIONS

A preliminary study of the system's response dependence on the coil's lift-off established that the detection limit to distinguish an aluminum sample from the background was equal to (2.0±0.1)cm and (1.5±0.1)cm for Q-factor and resonant frequency techniques, respectively.

Both resonant frequency and Q-factor imaging techniques were discovered to be valid methods to achieve 2D imaging of metallic samples. In particular, medium-high conductivity metals could be successfully imaged at values of capacitance equal to both C=(0.5000±0.0001)μF and C=(1.0000±0.0001)μF.

A comparison between the Q-factor and resonant frequency changes with conductivity highlighted the higher sensitivity of the Q-factor technique with respect to the resonant frequency one: ΔQ=[-11,-2]% vs Δf=[-0.3,0.7]%. Low-conductivity metals could be imaged with the resonant frequency technique only at certain values of capacitance; these are values that provided a sufficiently large change of resonant frequency from the background value. The range of suitability of the resonant frequency technique is therefore limited by material's conductivity. The Q-factor technique was found to be a powerful tool to overcome that constraint. Experimental results proved that this technique can accurately image any conductivity metal, irrespective of the external capacitance. Quantitative analysis made by using the Canny edge detection technique demonstrated that the Q-factor technique allows more accurate edge detection than the resonant frequency one. Results show that the ratio between detected edge and real edge increases with conductivity from 0.68 to 1 for all the tested non-magnetic materials. The resonant frequency technique leads to a systematic edge underestimation by a factor equal to 1.25 at C=(0.5000±0.0001)μF and 1.19 at C=(1.0000±0.0001)μF. Moreover, the edge estimation is independent from the sample's diameter in the range from 1.5 to 3 cm.

In conclusion, the possibility of distinguishing between metals having different values of conductivity is constraint by the small resonant frequency change on the one hand and the shape of the Q vs σ curve on the other hand. A valid method to achieve the desired goal of material characterization consists in applying the Q-factor technique by setting the lift-off to 0.5 cm. Further work will be carried out in order to investigate the dependence of the measured quantities from the material's susceptibility.

ACKNOWLEDGEMENTS

This research was funded by AWE and by UCL Impact Studentship scheme. We thank Soliman Edris for help with the Labview program.

REFERENCES

[1] Griffiths, H., "Magnetic induction tomography: a measuring system for biological tissues," Meas. Sci. Technol. 12, 1126-1131 (2001).
[2] Zolgharni, M., Griffiths, H. and Ledger, P.D., "Frequency-difference MIT imaging of cerebral haemorrhage with a hemispherical coil array: numerical modelling," Physiol. Meas. 31, S111-S125 (2010).
[3] Darrer, B. J., Watson, J. C., Bartlett, P. and Renzoni, F., "Magnetic Imaging: a New Tool for UK National Nuclear Security," Sci. Rep. 5 7944, 1-6 (2015).
[4] Peyton, A.J., Yu, Z.Z., Lyon, G., Al-Zeibak, S., Ferreira, J., Velez, J., Linhares, F., Borges, A.R., Xiong, H.L., Saunders, N.H. and Beck, M.S., "An overview of electromagnetic inductance tomography: description of three different systems," Meas. Sci. Technol. 7, 261-271 (1996).
[5] Wei, H.Y., Ma, L. and Soleimani, M., "Volumetric magnetic induction tomography," Meas. Sci. Technol. 23, 1-9 (2012).
[6] Wei, H.Y. and Soleimani, M., "A magnetic induction tomography system for prospective industrial processing applications," Chinese J. Chem. Eng. 20(2), 406-410 (2012).
[7] Gaydecki, P., Quek, S., Miller, G., Fernandes, B.T. and Zaid, M.A.M., "Design and evaluation of an inductive Q-detection sensor incorporating digital signal processing for imaging of steel reinforcing bars in concrete," Meas. Sci. Technol. 13, 1327-1335 (2002).
[8] Du, L., Zhu, X., Han Y., Zhao L. and Zhe J., "Improving sensitivity of an inductive pulse sensor for detection of metal wear debris in lubricants using parallel LC resonance method," Meas. Sci. Technol. 24(7), 1-10 (2013).

[9] Du, L. and Zhe J., "Parallel sensing of metallic wear debris in lubricants using undersampling data processing," Tribology International 53, 28-34 (2012).
[10] Weast, R.C., [Handbook of Chemistry and Physics], Boca Raton: CRC Press, 60th edition, Florida, E85-F172 (1979-1980).
[11] Canny, J.F., "A computational approach to edge detection," IEEE Transactions on pattern analysis and machine intelligence 8(6), 679-698 (1986).